Electrical and Electronic Conductivity of $CaO-SiO_2-FeO_x$ Slags at Various Oxygen Potentials: Part I. Experimental Results

MANSOOR BARATI and KENNETH S. COLEY

The oxygen potential dependences of total electrical and partial electronic/ionic conductivities for 'FeO'-$CaO-SiO_2$ slags have been studied both experimentally and theoretically in the present work. In the first part of this two-part article, the experimental results are presented for slags with 30 wt pct 'FeO' and CaO/SiO_2 wt ratios of 0.5, 1.0, and 2.0. For each slag composition, measurements of total electrical conductivity and electronic transference were made over a range of oxygen potentials and temperatures. The results were used to calculate the partial conductivities. A maximum was achieved in total and electronic conductances as a function of equilibrium CO_2/CO. The CO_2/CO corresponding to the maximum was shifted to lower values with increasing slag basicity (CaO/SiO_2 ratio). The other effect of basicity was increasing total and partial conductivities, with a magnitude that depends on oxygen potential and temperature. The activation energies for ionic and electronic conductances were in similar ranges and decreased with the basicity.

I. INTRODUCTION

THE electrical and electrochemical properties of oxide-containing melts have been the subject of a number of research studies of both fundamental and practical interest. The earliest of such studies were published in the middle of the twentieth century,[1–4] and increasing attention has been paid to the subject since then. The primary interest in studying the electrical properties of metallurgical slags is their application in the design and optimization of electric melting/smelting processes.

The electrical properties of metallurgical melts have also been of particular interest in the electrolytic production of metals. A large number of metals, including aluminum, magnesium, and titanium, have been produced by the electrolysis of molten slags and salts.[5,6]

In addition to their importance in industrial processes, the investigations of the electrical properties of slags have played a significant role in developing base knowledge about slags. Such studies were among the primary work through which insights into and an understanding of the structure of liquid oxides were developed. For example, the earliest evidence of the ionic structure of oxide melts resulted from electrical conductance measurements.[3,7–11]

Although oxide melts are regarded as ionic solutions, the electrical current in many of theses melts is conducted by both ionic and electronic charge carriers. The semiconduction behavior, or the contribution of electronic carriers in the conductivity of liquid FeO,[12,13] $FeO-SiO_2$,[14,15] FeO-CaO,[16] $FeO-CaO-SiO_2$,[17] $FeO-MnO-SiO_2$,[18] $FeO-CaO-MgO-SiO_2$,[19] TiO_2-BaO,[20,21] $PbO-SiO_2$,[22] and some molten salts,[23,24] has become evident in the last few decades. The relatively high conductance of many transition metal oxide melts has also been related to the electronic conduction mechanism in such melts.

The majority of the technological interest in understanding the electronic properties of slags arises from the fact that, for an efficient electrolysis, the melt must be predominantly an ionic conductor. Knowledge of the electronic conduction in slags can help in the design or selection of the proper slag for electrolysis,[21,25] or can be used in the optimization of furnace operation.[24]

From a more fundamental point of view, increasing attention has been paid to the electronic properties of molten slags, due to their significance in some reactions between gas or metal with slag. Some researchers have suggested that the reactions between slag and molten alloys are electrochemical in nature.[26–30] These findings, along with the evidence of the role of electrons in the mass transfer of oxygen through slag,[31,32] suggest that, for some reactions, the kinetics can be controlled by electronic transport in slag.

The relationship between the catalytic reaction of gases with solid oxides and the electronic structure of solids has been established for many years.[33–37] Several recent studies[38–41] have discussed that the reaction of iron oxide in liquid slag with $CO-CO_2$ gases involves the transfer of charge between the slag and the adsorbed gas species. In order to explore such reaction mechanisms, one needs to gain knowledge of the reaction kinetics and electronic properties of slag under similar conditions. The present authors have examined the oxidation-state dependence of the rate of CO_2 dissociation on different slags.[38] However, a very limited amount of data exist regarding the electronic properties of FeO_x-bearing slags. In particular, the dependence of the electronic properties, namely, the electronic conductivity, on the oxidation state of iron in slag has not been studied at all. The objective of this work was to study the dependence of the electrical and electronic conductivity of FeO_x-containing slags in order to (1) clarify any relationship between the kinetics of iron oxide oxidation/reduction in slag and its electronic properties and (2) stimulate similar studies for both academic and applied interests. Thus, both an experimental

MANSOOR BARATI, former Ph.D. student, McMaster University, is currently with WP HG Engineering, Toronto, Ontario, Canada. KENNETH S. COLEY, Associate Professor, is with Department of Materials Science and Engineering, McMaster University, Hamilton, Ontario, Canada L8S 4L7. Contact e-mail: coleyk@mcmaster.ca

Manuscript submitted June 11, 2005.

and a theoretical analysis were undertaken on the equilibrium-oxygen-pressure dependence of electrical and electronic conductivities. In the first part of this two-part series, the experimental method and results are presented. In the second part, the results will be analyzed quantitatively and a model for electronic conduction will be presented, with an emphasis on the mechanism of conduction.

II. EXPERIMENTAL DETAILS

A. *Principles of Measurements*

Iron-oxide-containing slags can be regarded as mixed conductors, since they exhibit both ionic and electronic conductivity, as discussed in Section I. For these materials, the transference numbers of different carriers are defined, to quantify the relative significance of each type of charged particle in the overall conduction. For a mixed conductor, electronic (t_e) and ionic (t_i) transference numbers are defined as

$$t_e = \frac{i_e}{i_e + i_i} \quad [1]$$

$$t_i = \frac{i_i}{i_e + i_i} \quad [2]$$

where i_e and i_i are the currents carried by the electronic and ionic charge carriers, respectively.

In ohmic conduction through a mixed ionic-electronic conductor, the applied voltage to all charge carriers is identical. Also, the current paths are similar for both the ionic and electronic modes of conduction, provided that the charged particles are distributed homogeneously, throughout the material. Therefore, one can correlate transference numbers to the partial ionic and electronic conductivities as

$$t_e = \frac{\sigma_e}{\sigma_t} \quad [3]$$

and

$$t_i = \frac{\sigma_i}{\sigma_t} \quad [4]$$

where σ_e and σ_i represent electronic and ionic conductivity, respectively. Total conductivity is given by

$$\sigma_t = \sigma_e + \sigma_i \quad [5]$$

Therefore, the correlation between t_e and t_i can be obtained as

$$t_e + t_i = 1 \quad [6]$$

As seen from these equations, the electronic and ionic conductivities can be calculated if the both total conductance and the electronic (or ionic) transference numbers are known.

The total electrical conductivity in this study was calculated by Eq., from the total resistance (R) of the slag layer between the electrodes, using an alternating current (AC) signal at proper frequency, as follows:

$$\sigma_t = G/R \quad [7]$$

The G in Eq. is the geometry factor (or cell constant); it is related to the length (l) and cross-sectional area (A) of the current path, as shown in Eq.:

$$G = l/A \quad [8]$$

The stepped potential chronoamperometry (SPC) method was employed in the present work for the measurement of the transference numbers. The SPC technique was recently introduced by Fried,[20,21] initially for the determination of the transference number in TiO_2-BaO melts; it was later also used for FeO-CaO-MgO-SiO_2 slags.[19] The method has already been used for polymers,[42,43,44] solid electrolytes,[45] and mixed-oxide conductors. Basically, in this technique, the current response upon applying a constant voltage (stepped potential) is monitored as a function of time. The electronic transference number can then be calculated from the initial ($i_{t\to 0}$) and long-time ($i_{t\to\infty}$) values of the current, using Eq.:

$$t_e = \frac{i_{t\to\infty}}{i_{t\to 0}} \quad [9]$$

For physical phenomena, when the potential is applied to a mixed conducting material placed between two ion-blocking electrodes, polarization occurs at the electrode/sample interfaces and ions become stationary at their positions, after a sufficiently long time ($t \to \infty$). After this time, further conduction will be caused by the movement of more mobile electronic carriers, and the decay of the current to a fixed value indicates the variation in the conduction mode from mixed to purely electronic. An example of such measurements is shown in Figure 1.

B. *Experimental Setup and Procedure*

1. *Experimental setup*

A four-terminal technique was employed for the measurements in the present study. The method requires the immersion of four high-temperature-resistant, inert conducting rods, which serve as electrodes, into the slag. The

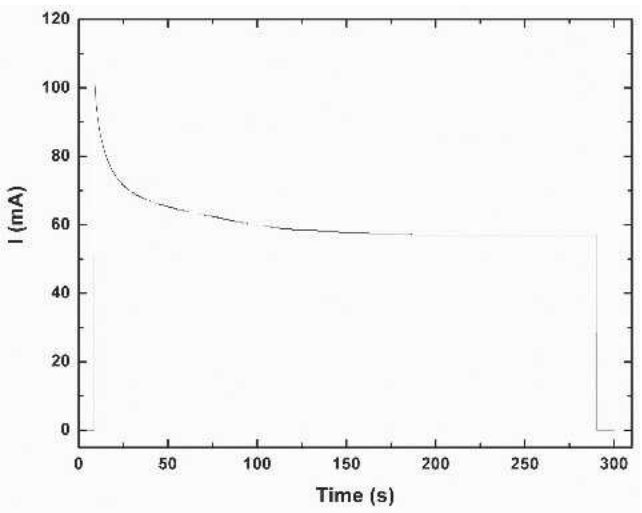

Fig. 1—A typical current decay curve created due to the application of a stepped potential.

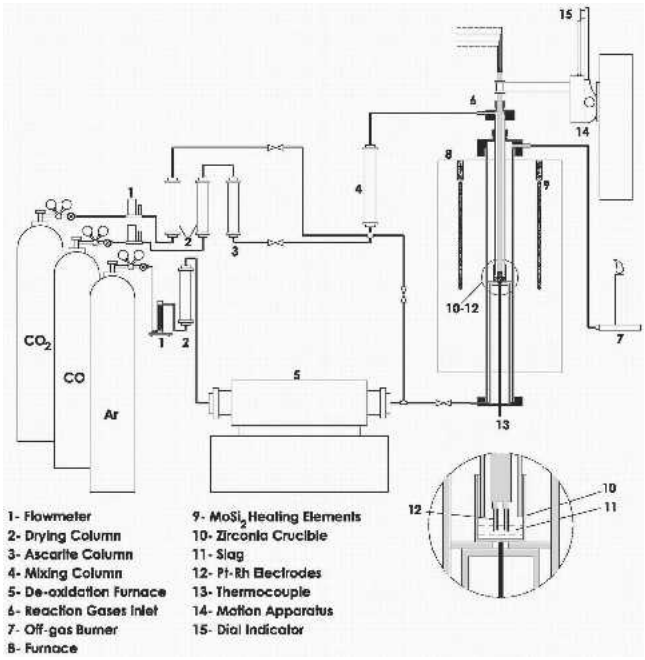

Fig. 2—Schematic of experimental arrangement, including furnace and electrode motion apparatus.

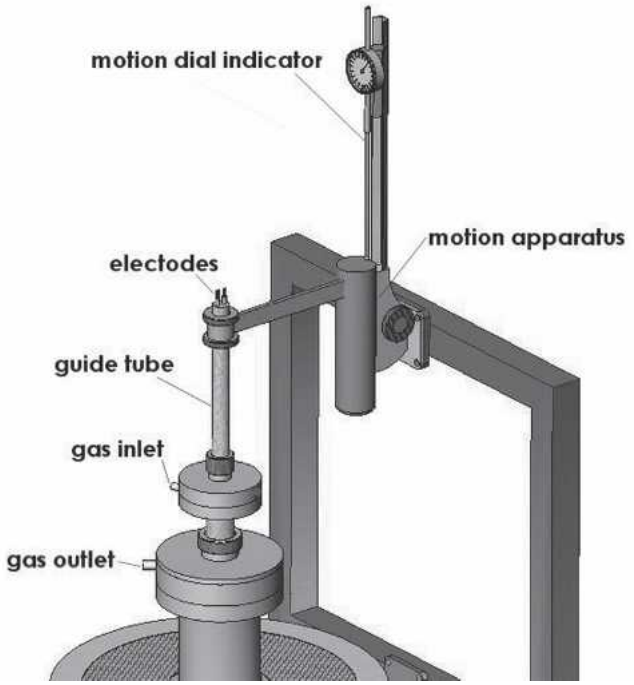

Fig. 3—Schematic drawing of the furnace top and motion apparatus connected to the electrodes guide.

experimental arrangement is drawn schematically in Figure 2. A high-temperature-resistance heating furnace with an 80-mm diameter alumina working tube was employed in the experiments. The top construction of the furnace was designed to accommodate the electrodes and their immersion control apparatus.

The electrodes were made from Pt-(30 wt pct) Rh. Each electrode consisted of a tip (25 mm long and 0.81 mm in diameter) welded to a thinner extension wire (of the same material, but 0.25 mm in diameter and 800 mm long). The electrodes were sheathed into two twin-bore alumina tubes, so that the tips were extended about 20 mm outside the tubes. The tubes were then passed down a support tube (13-mm ID) and, using alumina cement, they were stabilized rigidly, so that the two central electrodes were fixed 7 mm apart. The support tube extended outside the furnace and attached to the immersion control apparatus. Gas was passed down a larger tube, co-centered with the support tube.

In order to accurately determine the cell factor (G), the electrode immersion depth must be monitored carefully. For this purpose, a special motion-control device was constructed and installed on the top of the furnace. This device had a 50-mm stroke and could be moved up or down by rotating a knob. A motion dial indicator was mounted on the stationary part of the stage, for measurement of the displacement. Any vertical movement could be shown on the dial face with the precision of 0.0254 mm. Figure 3 shows the top arrangement of the furnace and the details of the motion apparatus.

2. *Cell calibration*

Cell calibration for determination of G was performed at low temperatures (16 °C to 20 °C), using standard aqueous KCl solutions. Standard 0.01D, 0.1D, and 1.0D (Demal) solutions were used for calibration, as their preparation[46,47] and specific conductance[48,49,50] were well documented.

Table I. Initial Composition of Slag Samples

Slag (Wt Pct)	'FeO'	CaO	SiO_2	C/S
A	30	23.33	46.67	0.5
B	30	35.00	35.00	1.0
C	30	46.67	23.33	2.0

The measurement of electrical resistance was carried out with the same equipment used for measuring the resistance of slag. The resistance was essentially independent of frequency, from 1 to 100 kHz. The total resistance was measured as a function of the immersion depth of the electrodes and was used in Eq. to determine G.

3. *Experimental procedure*

Three slag compositions, identified as A, B, and C, were made by mixing laboratory reagent-grade CaO, SiO_2, and Fe_2O_3 powders. The iron oxide content in the slags was maintained at 30 wt pct and the CaO/SiO_2 ratio varied between 0.5 and 2 (wt ratio). The initial slag compositions are provided in Table I.

Slag samples were made by melting each powder mix in a platinum crucible in air, using a muffle furnace. The molten slag was quenched on a thick steel plate and ground to fine powder. A cylindrical crucible was used to maintain 8 to 10 g of slag at high temperature. Zirconia was used as the material of the crucible, since it has the dual advantage of having both low conductivity (thus minimizing current leakage through crucible walls) and a low level of dissolution in the slag. The crucible was then placed at the proper position inside the furnace, where the temperature variations were negligible, in a 4-cm height. The bottom end of the gas-conducting tube was then positioned about 0.5 to 1 cm above the melt. Before melting the slag, the tips of the electrodes were located

at about 2 cm above the surface. The furnace temperature was then raised to the target temperature, with argon gas flowing over slag during the heat-up. The furnace temperature was automatically controlled by a programmable EUROTHERM (Leesburg, VA) controller, and the temperature measurement was carried out using a type B (Pt-6 pct Rh/Pt-30 pct Rh) thermocouple in contact with the bottom of the crucible. Once the final temperature was reached, 1 hour was allowed, to ensure the melting and homogenization of the slag. The electrodes were then lowered very slowly until they touched the surface of the melt. The first contact of the electrodes with the melt was noted with a sharp decrease in the resistance. The electrodes were lowered further to reach to the desired depth. In all experiments, the initial immersion depth of the electrodes was 2.54 mm. The electrodes were left at the same level for the duration of the experiment. This immersion depth, as estimated from the calibration curve, yields a cell constant of approximately 1.6 cm^{-1}.

After the immersion of the electrodes, the slag was exposed to a gas mixture of Ar-CO-CO_2, with a controlled flow rate and CO_2/CO ratio. The input gas composition varied from pure CO_2 to $CO_2/CO = 0.5$. The total flow rate of CO and CO_2 was fixed at 600 N cm^3/min. Argon was added at 200 to 300 N cm^3/min, to all gas mixtures except pure CO_2. Each experiment started at 1750 K and flowing pure CO_2. The continuous measurement of resistance allowed the determination of the equilibrium time. This was defined as the time when the measured resistance became stable. The equilibrium was achieved in about 1 to 2 hours, depending on the slag and the gas composition. Once the slag and gas reached equilibrium, the electrical measurements were carried out. Afterward, the gas atmosphere or the temperature was changed and the steps were repeated.

4. *Electrical measurements*

The slag resistance was measured using a Model PM 6304 Fluke Programmable RCL meter. The resistance of the slag layer between electrodes was automatically calculated by the equipment, from the total measured impedance. In the beginning of each experiment, the resistance was measured at the frequencies ranging from 50 Hz to 100 kHz. The resistance was found to be independent of the frequency, over the range 1 to 100 kHz. All of the measurements were therefore carried out at 20 kHz.

The electronic transference number was measured by the SPC method, using a direct current (DC) signal. A Model 273 potentiostat/galvanostat (Princeton Applied Research, Oak Ridge, TN) was employed for the DC measurements. The potentiostat was used to generate a square wave by turning the applied voltage on and off at the desired times. The experiment was started in the open circuit condition, followed by an applied potential of 0.2 V for 3 to 4 minutes. Once the current reached a steady-state value, the potentiostat was switched back to the open circuit. The current was recorded during the experiment at 0.1-second time intervals. A typical current decay curve obtained from the DC measurements is shown in Figure 1. The initial peak and final stable currents were used to calculate the electronic transference numbers.

III. RESULTS

The electrical conductivity and electronic transference numbers for the slags studied in this work were calculated from Eqs. and , respectively. The value of the cell constant (G) was determined by calibrating the cell with standard solutions. The partial electronic and ionic conductivities were calculated using Eqs. and , respectively. The estimated errors for total and partial conductivities were 3 and 6 pct, respectively.

This article is Part I of a two-part series; it presents the results of measurements and compares them with similar studies. In Part II of the series, the results will be analyzed quantitatively, with an emphasis on the details of the mechanism of conduction.

A. *Total Electrical Conductivity*

1. *Effect of equilibrium oxygen potential and slag basicity*

Figure 4 shows the electrical conductivity at 1750 K of three slags as a function of equilibrium oxygen potential, expressed as a CO_2/CO ratio. As seen, for slags with CaO/SiO_2 ratios of 1.0 and 2.0, increasing the oxygen potential first increases and then decreases the electrical conductivity. For the slag with a C/S = 0.5, the curve did not reach a maximum, as the imposed oxygen potential had probably not been high enough. Similar trends in the variation of conductivity with oxygen potential have been reported by other authors.[51–55]

Increasing the slag basicity expressed as a C/S ratio reveals two significant effects: (1) it increases the magnitude of the electrical conductivity significantly and (2) the CO_2/CO ratio at which the electrical conductivity is at a maximum value, $(CO_2/CO)_{\sigma_{max}}$, is shifted to lower values.

Figure 5 compares the electrical conductivity data from this work and the results reported by Fontana *et al.*[54] and Hundermark *et al.*,[56] for slags with approximately similar iron oxide content. The oxygen partial pressures in this figure were calculated from the equilibrium constant of reaction $CO_2 = CO + 1/2O_2$. The iron oxide content in this work is identical to the results reported by Hundermark *et al.*, but their slag contained MgO and Al_2O_3 in addition to CaO and SiO_2. A good agreement between the two sets of data

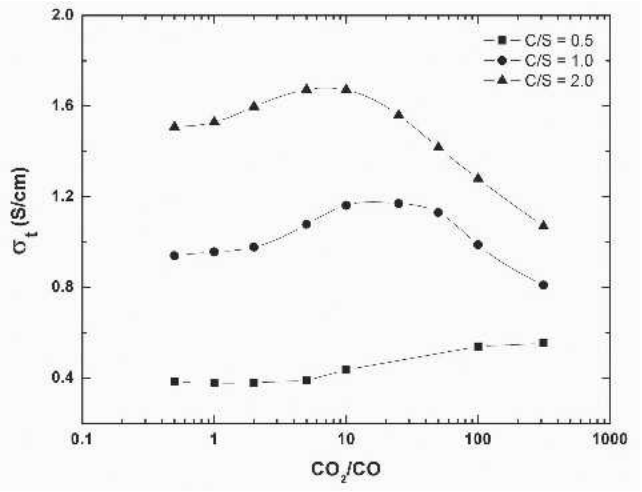

Fig. 4—Total electrical conductivity, as a function of the equilibrium CO_2/CO ratio, at 1750 K.

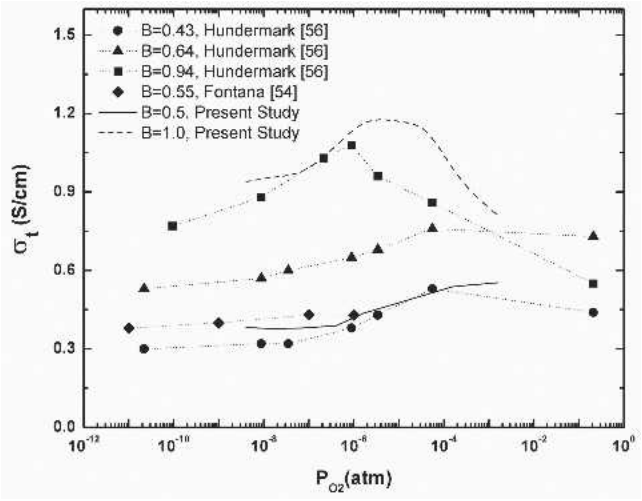

Fig. 5—Electrical conductivity as a function of oxygen partial pressure. The results from Hundermark *et al*. are for 30 wt pct 'FeO' + (CaO-SiO_2-MgO-Al_2O_3) melts at 1723 K. The results taken from Fontana *et al*. are for ~30 wt pct 'FeO' + (CaO-SiO_2-MgO-Al_2O_3) at 1623 K. The basicity index B in the legend is equal to the (CaO + MgO)/(SiO_2 + Al_2O_3) wt ratio.

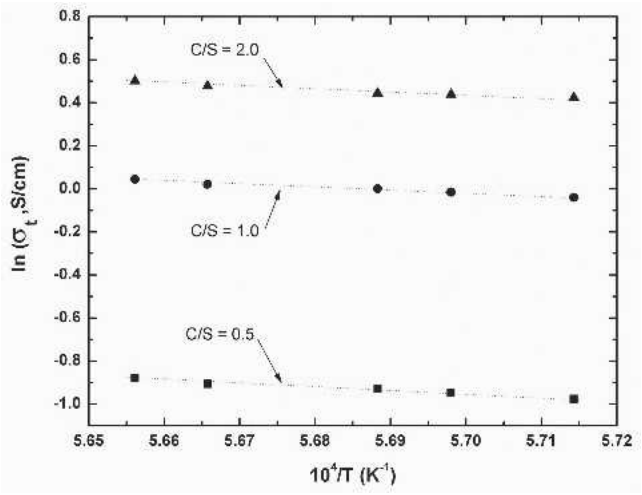

Fig. 6—Arrhenius plot of electrical conductivity for slags A through C, at CO_2/CO = 1.0.

for approximately equal (CaO + MgO)/(SiO_2 + Al_2O_3) is seen.

2. *Effect of temperature on the electrical conductivity*

The electrical conductivity was measured at unit CO_2/CO for three slags, as a function of temperature. Figure 6 shows that at unit CO_2/CO, basicity has a greater influence on the total conductivity in the range of C/S = 0.5 to 1, compared to that of C/S = 1.0 to 2.0. As seen in this figure, an Arrhenius-type relation is followed, from which the apparent activation energy of total conduction can be calculated. The apparent activation energy of total conductivity for slags A, B, and C are 129, 113, and 108 kJ/mol, respectively. These values are compared with some previous measurements in Figure 7. A good agreement is observed for relatively similar slag compositions. Iron oxide content, as shown in this figure, has a significant effect on the lowering of the activation energy.

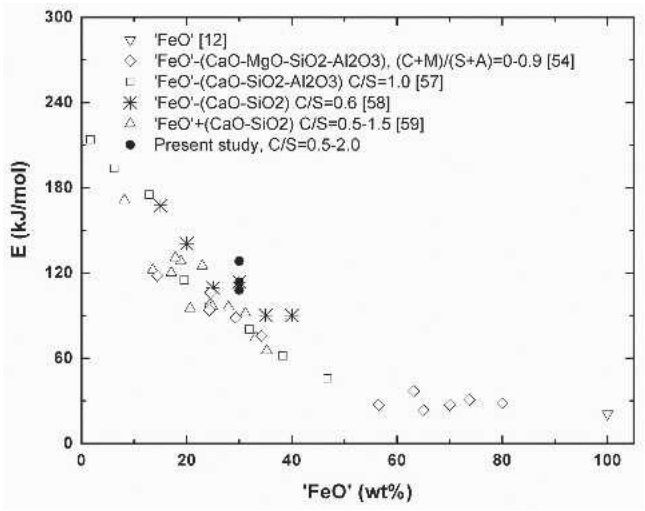

Fig. 7—Activation energy of total conductivity, as a function of iron oxide content.

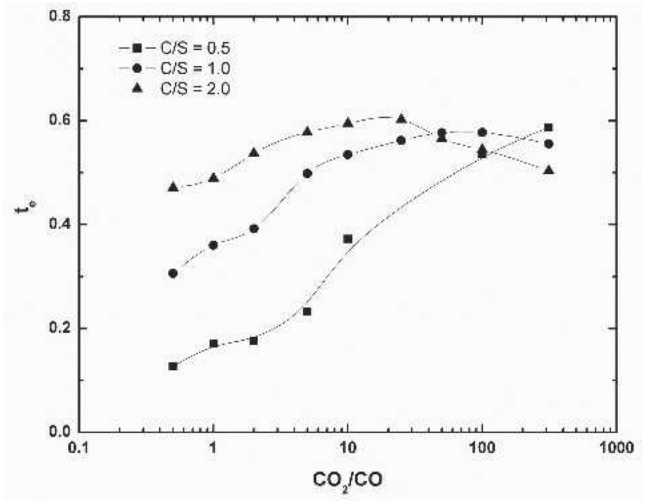

Fig. 8—The dependence of electronic transference on equilibrium CO_2/CO, at 1750 K.

B. *Electronic Transference Number*

1. *Effect of equilibrium oxygen potential and slag basicity*

The electronic transference number is shown as a function of CO_2/CO, for different slags in Figure 8. It can be seen that, depending on slag composition and equilibrium CO_2/CO ratio, the fraction of current delivered by electronic carriers varies from about 10 to 60 pct. At low CO_2/CO, for slags with C/S = 0.5, the t_e is smaller than for more basic slags. However, increasing the oxygen potential gives a marked increase in the t_e for this slag. The increasing trend is followed, up to the maximum CO_2/CO ratio considered in this study. The t_e of the other two slags, on the other hand, shows less variation with oxygen potential and exhibits a maximum at a certain CO_2/CO.

No data are available in the literature for the dependence of the t_e on the oxidation state of slags. Therefore, a direct comparison with the present results cannot be made.

However, Figure 9 shows that, for the melts in equilibrium with iron, the t_e is higher in the more basic slags at a given iron oxide content, which is consistent with the current work.

2. *Effect of temperature*

The electronic transference number was measured under conditions identical to those of the electrical conductivity measurements. The results are provided in Figure 10. It is evident from this figure that, at unit CO_2/CO, basicity has a marked effect on the t_e, particularly in the range of basicity from 0.5 to 1.0. The data show that, in the range of experimental conditions, the t_e is essentially independent of the temperature, for each slag. The negligible effect of temperature on the transference number has also been observed for FeO_x-SiO_2,[15] CaO-FeO_x,[16] and FeO-CaO-SiO_2[17] melts.

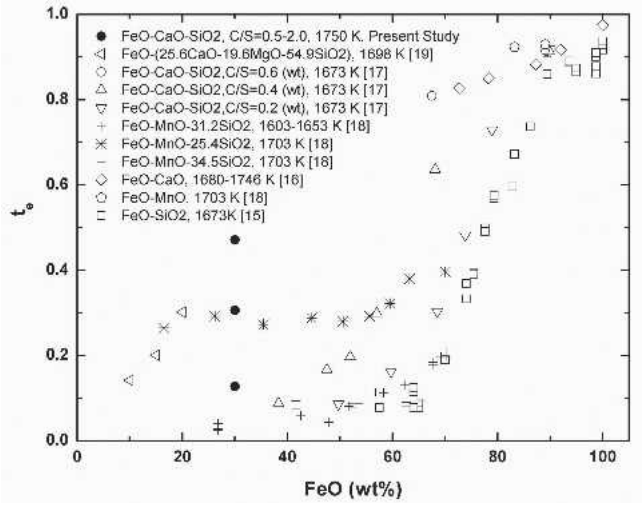

Fig. 9—The electronic transference number of some FeO_x-containing melts. The results taken from Refs. through to were calculated from current efficiency measurements. Slag compositions are reported in wt pct.

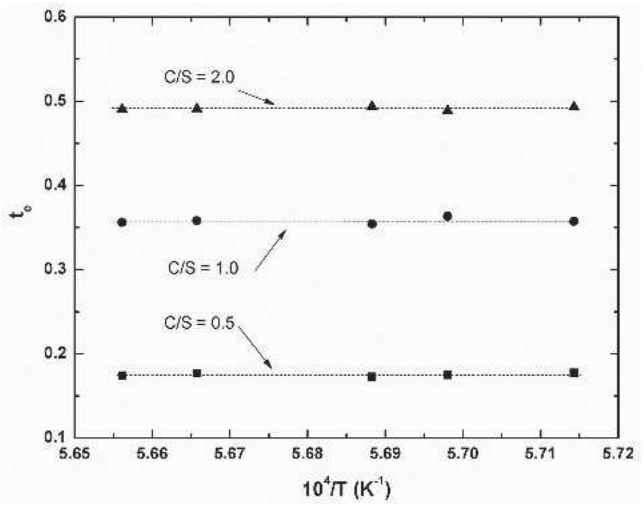

Fig. 10—The electronic transference number as a function of temperature, at $CO_2/CO = 1.0$.

Supposing that both ionic and electronic conductance correlate with temperature through the equation

$$\sigma = \sigma^{\circ}\exp(-E/RT) \quad [10]$$

one can combine this equation with Eq. to obtain

$$t_e = \frac{\sigma_e^{\circ}\exp(-E_e/RT)}{\sigma_e^{\circ}\exp(-E_e/RT) + \sigma_i^{\circ}\exp(-E_i/RT)} \quad [11]$$

Based on Eq., the effect of temperature on the t_e becomes negligible only if the activation energies of ionic and electronic conduction lie in a similar range. The reason for this will be explored in Part II of the series.

Figures 11 and 12 and show the effect of temperature on the electronic and ionic conductivity. Generally, both partial conductivities follow an Arrhenius-type expression. The values of the activation energy for ionic, electronic, and total conductivity are given against a CaO/SiO_2 ratio in Figure 13. As expected from the earlier discussion, and as

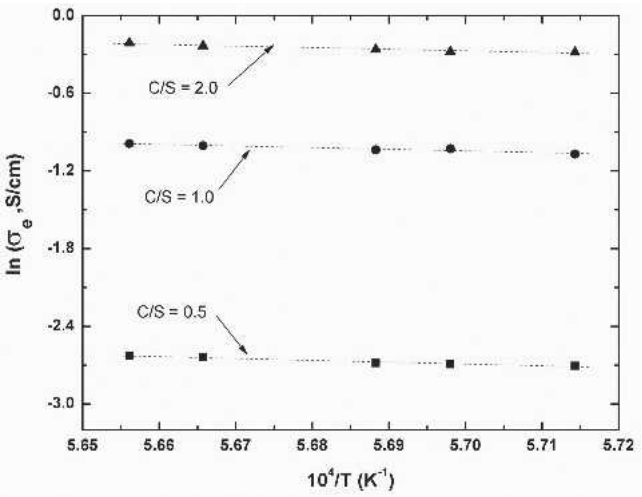

Fig. 11—Arrhenius plot of electronic conductivity, at $CO_2/CO = 1.0$.

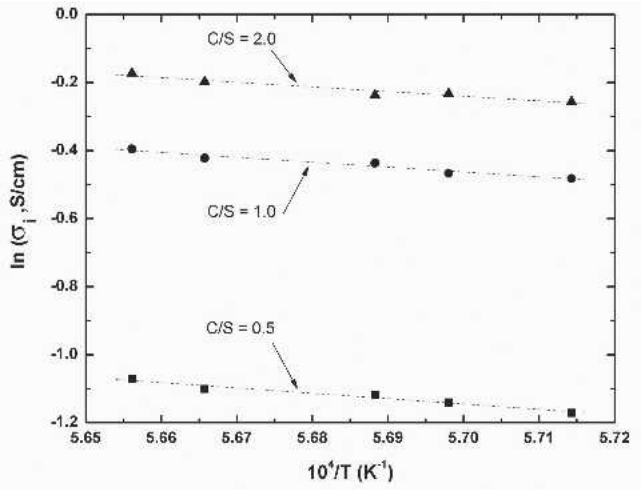

Fig. 12—Arrhenius plot of ionic conductivity, at $CO_2/CO = 1.0$.

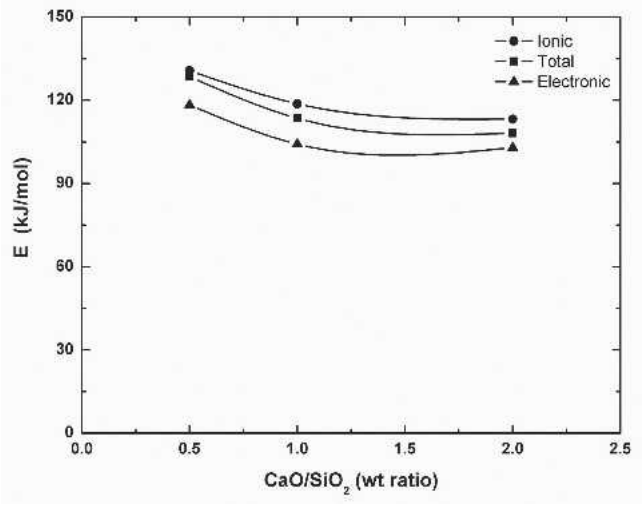

Fig. 13—The activation energy of partial and total electrical conductivities, at $CO_2/CO = 1.0$.

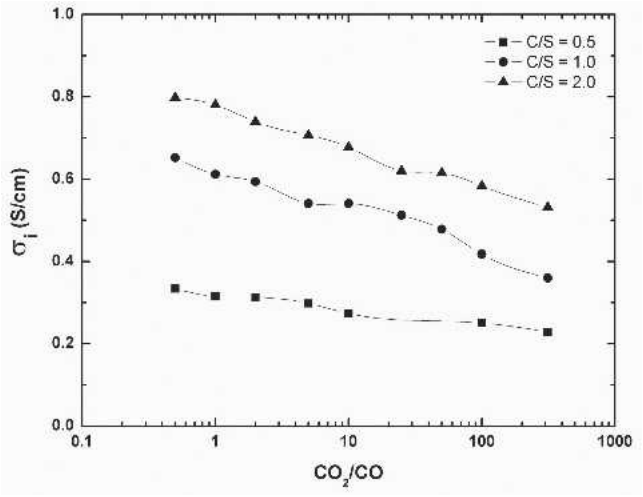

Fig. 14—Ionic conductivity as a function of equilibrium CO_2/CO, at 1750 K.

is also evident from Figure 13, both E_e and E_i are relatively close to each other, and both decrease with the melt basicity.

C. *Effect of Equilibrium Oxygen Potential and Slag Basicity on Ionic Conductivity*

Figure 14 shows the dependence of ionic conductivity on the equilibrium oxygen potential, expressed as CO_2/CO. As seen, for slags A, B, and C, the ionic conductance declines with increasing CO_2/CO.

D. *Effect of Equilibrium Oxygen Potential and Slag Basicity on Electronic Conductivity*

The values of electronic conductivity at 1750 K are plotted against the CO_2/CO ratio, in Figure 15. With a lower magnitude, the variations follow similar trends to total conductivity. The P_{O_2} corresponding to the maximum conductivity are 1.6×10^{-3}, 1.0×10^{-5}, and 4.0×10^{-7} atm, for slags with CaO/SiO_2 ratios of 0.5, 1.0, and 2.0, respectively.

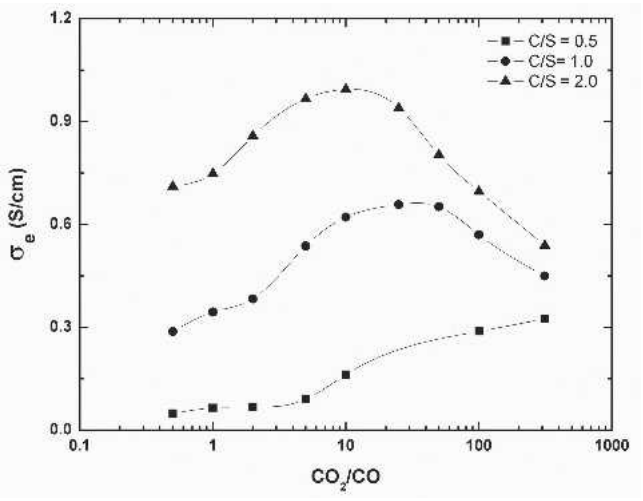

Fig. 15—Electronic conductivity as a function of equilibrium CO_2/CO, at 1750 K.

IV. DISCUSSION

As all the measurements were carried out in equilibrium conditions between the slag and the gas, the dependence of both the ionic and the electronic conductivity can be related to the change in oxidation state of iron ions, corresponding to the following reaction:

$$FeO + CO_2 \rightleftharpoons FeO_{1.5} + CO_2 \qquad [12]$$

In Figure 14, it was shown that the ionic conductance of all slags decreased, as a function of oxygen potential. The equilibrium described earlier suggests that this can be related to the replacement of ferrous with ferric ions, at the higher CO_2/CO ratios. It has been assumed by different authors[53,54] that Fe^{2+} is the only iron ion that significantly contributes to the ionic conduction in iron-oxide-containing melts. The increase in the ionic conductivity from slags A through C can be discussed in terms of two phenomena: (1) primarily, with the increase in the CaO/SiO_2 ratio, the concentration of mobile calcium cations is increased in the slag and (2) moreover, the addition of CaO, decreases the viscosity of slag by the depolymerization of the silicate network, which also brings about the higher mobility of the ionic charge carriers.

The effect of the slag oxidation state on the electronic conductivity is explained by considering the mechanism of semiconduction in solid iron oxide. The general agreement in the literature is that both wustite and magnetite exhibit p-type semiconductor behavior at high temperatures. (For a comprehensive review on the electrical and electronic properties of iron oxides, refer to Gleitzer.[60]) The mechanism of electronic conduction has been discussed as an activated charge hopping between ferric and ferrous ions. In this mechanism, an electron, provided with the thermal excitations, can jump from the low-valence to the high-valence ion. This mechanism of conduction, referred to as "small polaron hopping," has also been suggested for transition metal oxide glasses,[61] and can be used to explain the results of the present study. Electronic conduction *via* charge hopping requires neighboring divalent and trivalent iron ions to interact. Increasing the oxygen potential increases the fraction of the electron acceptor sites (Fe^{3+}), at the expense of decreasing the fraction of

the charge-donating sites (Fe^{3+}). As a result, increasing the P_{O_2} to a certain extent increases the number of adjacent $Fe^{3+} - Fe^{2+}$ couples and, hence, promotes the electronic conduction. Further oxidation of the slag decreases this number and lowers the electronic conductivity. This explanation justifies increasing and then decreasing the electronic conductivity *vs* P_{O_2}, in Figure 15. The effect of the bulk composition of the slag on electronic conductivity can also be interpreted in terms of its influence on the distribution of iron between the trivalent and divalent states. For example, due to a higher Fe^{3+}/Fe^{2+} ratio in the more basic slags, lower oxygen potentials are required in order to reach maximum conductivity.

The positive effect of temperature on ionic conductivity can be related to the increased mobility of cations at higher temperature, due both to a greater diffusion coefficient and to more depolymerization of the silicate structure. As was shown in Figure 13, the activation energy of the electronic conductivity is very close to that of the ionic conductivity. The values are, however, much larger than the typical activation energies measured for electronic conduction in oxide materials that are about 30 to 40 kJ/mol.[62] The differences indicate that, if a small polaron, hopping as indicated earlier, dominates the electronic conduction, its detailed mechanism is different in the liquid slag and the solid materials. This subject will be discussed in more detail in Part II of the series.

V. CONCLUSIONS

1. The measurement of electrical conductivity and electronic transference numbers were made as a function of oxygen potential, for slags with 30 wt pct FeO and a CaO/SiO_2 ratio between 0.5 and 2.0.
2. The electronic transference number exhibits a strong dependence on both oxygen potential and slag basicity, while it is essentially independent of temperature.
3. The ionic conductivity increased as a function the CaO/SiO_2 ratio, presumably because of a higher concentration of Ca^{2+} cations and decreased slag viscosity.
4. The effect of oxygen potential on electronic conductivity is suggestive of a small polaron-hopping mechanism between Fe^{2+} and Fe^{3+}; this suggests, in turn, that the electronic conductivity will reach its maximum when both cations present at approximately equal concentrations. The magnitude of the activation energy, however, is larger than the typical activation energies measured for this mechanism of conduction in solid oxides.
5. The activation energies of the ionic and the electronic conductivities are in similar ranges, and both are decreased with increasing CaO/SiO_2 in the slag.

ACKNOWLEDGMENTS

The authors greatly appreciate the useful discussions and suggestions by Professors J. Deen and G.A. Irons. The authors also acknowledge McMaster Steel Research Centre for funding the project.

REFERENCES

1. A. Wenjarth: *Trans. Electrochem. Soc*., 1934, vol. 65, pp. 177-87.
2. A. Wenjarth: *Trans. Electrochem. Soc*., 1934, vol. 65, pp. 329-43.
3. A.E. Martin and G. Derge: *Trans. AIME*, 1943, vol. 154, pp. 104-15.
4. C. Wagner and E. Koch: *Z. Phys. Chem. B*, 1936, vol. 22, p. 439.
5. R. Winand: *Proc. Conf. Extraction Metallurgy 81*, IMM, London, 1981, pp. 20-33.
6. D.R. Sadoway: U.S. Patent No. 5,185,068, 1993.
7. J. Chipman and L.C. Chang: *Trans. AIME*, 1949, vol. 185, pp. 191-97.
8. J.O'M. Bockris and J.W. Tomlinson: *Research*, 1949, vol. 2, pp. 362-68.
9. J.O'M. Bockris, J.A. Kitchener, S. Ignatowicz, and J.W. Tomlinson: *Trans. Faraday Soc*., 1952, vol. 48, pp. 75-91.
10. P. Harasymenko: *Trans. Faraday Soc*., 1938, vol. 34, pp. 1245-57.
11. P. Harasymenko and G.E. Speight: *J. Iron Steel Inst*., 1950, vol. 166, pp. 169-83.
12. H. Inouye, J.W. Tomlinson, and J. Chipman: *Trans. Faraday Soc*., 1953, vol. 49, pp. 796-801.
13. J.W. Tomlinson and H. Inouye: *J. Chem. Phys*., 1952, vol. 20, no. 1, p. 193.
14. M.T. Simnad and G. Derge: *J. Chem. Phys*., 1953, vol. 21, no. 5, pp. 933-34.
15. M.T. Simnad, G. Derge, and I. George: *Trans. AIME*, 1954, vol. 200, pp. 1386-90.
16. E.A. Dancy and D.J. Derge: *Trans. AIME*, 1966, vol. 236, pp. 1642-48.
17. W.R. Dickson and E.B. Dismukes: *Trans. AIME*, 1962, vol. 224, pp. 505-11.
18. D.A. Dukelow and G. Derge: *Trans. AIME*, 1960, vol. 218, pp. 139-40.
19. A. Ducret, D. Khetpal, and D.R. Sadoway: *Proc. 13th Int. Symp. on Molten Salts*, H.C. Delong, R.W. Bradshaw, M. Matsunaga, G.R. Stafford, and P.C. Trulove, eds., The Electrochemical Society, Pennington, NJ, 2002, pp. 347-53.
20. N.A. Fried, G.K. Rhoads, and D.R. Sadoway: *Electrochim. Acta*, 2001, vol. 46, pp. 3351-58.
21. N.A. Fried: Ph.D. Thesis, Massachusetts Institute of Technology, Cambridge, MA, 1995.
22. U.D. Pal, T. DebRoy, and G. Simkovich: *Metall. Trans. B*, 1985, vol. 16B, pp. 77-82.
23. G.M. Haarberg, K.S. Osen, R.J. Heus, and J.J. Egan: *J. Electrochem. Soc*., 1990, vol. 137 (9), pp. 2777-81.
24. G.M. Haarberg, K.S. Osen, J. Thonstad, R.J. Heus, and J.J. Egan: *Metall. Trans. B*, 1993, vol. 20B, pp. 728-35.
25. S.L. Schiefelbein: Ph.D. Thesis, Massachusetts Institute of Technology, Cambridge, MA, 1996.
26. K.G. Leewis, W.F. Caley, and C.R. Masson: *Proc. 2nd Int. Symp. on Metallurgical Slags and Fluxes*, H.A. Fine and D.R. Gaskell, eds., TMS-AIME, Warrendale, PA, 1984, pp. 685-97.
27. G.G. Krishna Murthy, A. Hasham, and U.D. Pal: *Ironmaking and Steelmaking*, 1993, vol. 20, no. 3, pp. 191-200.
28. U.B. Pal and D.R. Sadoway: U.S. Patent No. 5,632,800, 1997.
29. D.E. Woolley and U.D. Pal: *Metall. Mater. Trans. B*, 1999, vol. 30B, pp. 877-89.
30. D.E. Woolley and U.D. Pal: *Ironmaking and Steelmaking*, 2002, vol. 29 (2), pp. 125-32.
31. J.L. Speelman, W.F. Caley, and K.G. Leewis: *Metall. Trans. B*, 1989, vol. 20B, pp. 31-37.
32. M. Sasabe and A. Asamura: *Proc. 2nd Int. Symp. on Metallurgical Slags and Fluxes*, H.A. Fine and D.R. Gaskell, eds., TMS-AIME, Warrendale, PA., 1984, pp. 651-67.
33. O.V. Krylov: *Catalysis by Nonmetals*, Academic Press, New York, NY, 1970.
34. G. Parravanao: *Catal. Rev*., 1970, vol. 4 (1), pp. 53-76.
35. G. Parravanao: *Proc. Symp. on Electronic Phenomena in Chemisorption and Catalysis on Semiconductors*, K. Hauffe and T.H. Wolkenstein, eds., Moscow, 1968, pp. 111-22.
36. K. Hauffe: *Adv. Catal. Rel. Subj*., 1955, vol. 7, pp. 213-57.
37. T.H. Wolkenstein: *Adv. Catal. Rel. Subj*., 1960, vol. XII, pp. 189-264.
38. M. Barati and K.S. Coley: *Metall. Mater. Trans. B*, 2005, vol. 36B, pp. 169-78.
39. Y. Li and I.P. Ratchev: *Metall. Mater. Trans. B*, 2002, vol. 33B, pp. 651-60.
40. S.K. EL-Rahaiby, Y. Sasaki, D.R. Gaskell, and G.R. Belton: *Metall. Trans. B*, 1986, vol. 17B, pp. 307-16.
41. Y. Sasaki, S. Hara, D.R. Gaskell, and G.R. Belton: *Metall. Trans. B*, 1984, vol. 15B, pp. 563-71.
42. J. Evans, C.A. Vincent, and P.G. Bruce: *Polymer*, 1987, vol. 28, pp. 2324-28.
43. P.G. Bruce and C.A. Vincent: *J. Electroanal. Chem. Interfacial Electrochem*., 1987, vol. 225, pp. 1-17.

44. P.G. Bruce, C.A. Vincent, and J. Evans: *Solid State Ionics*, 1988, vol. 28/30, pp. 918-22.
45. Y.C. Yeh, T.Y. Tseng, and D.A. Chang: *J. Am. Ceram. Soc*., 1990, vol. 73, no. 7, pp. 1992-98.
46. G. Jones and B.C. Bradshaw: *J. Am. Ceram. Soc*., 1933, vol. 55, pp. 1780-1800.
47. G.J. Janz and R.P.T. Tomkins: *J. Electrochem. Soc*., 1977, vol. 124, p. 55C.
48. Y.C. Wu, W.F. Koch, W.J. Hamer, and R.L. Kay: *J. Solution Chem*., 1987, vol. 16, pp. 985-97.
49. Y.C. Wu, K.W. Pratt, and W.F. Koch: *J. Solution Chem*., 1989, vol. 18, pp. 515-28.
50. Y.C. Wu and W.F. Koch: *J. Solution Chem*., 1991, vol. 20, pp. 390-401.
51. T. Tran, S. Sun, and S. Jahanshahi: *Proc. 5th Int. Conf. Molten Slags, Fluxes and Salts*, Iron and Steel Society AIME, 1997, pp. 115-23.
52. R.J. Hundermark, S. Jahanshahi, and S. Sun: *Proc. 7th Int. Conf. Molten Slags, Fluxes and Salts*, Cape Town, South Africa, 2004, South African Institute of Mining and Metallurgy, Johannesburg, South Africa, pp. 487-93.
53. H.J. Engell and P. Vygen: *Berichte Bunsengesellschaft*, 1968, vol. 72 (1), pp. 5-11.
54. A. Fontana, K. Segers, K. Twite, and R. Winand: *TMS-AIME Papers Selection*, TMS-AIME, Warrendale, PA, 1984, Metallurgical Society of AIME, Littleton, CO, paper no. A84-39.
55. E.A. Pastukhov, O.A. Esin, and S.K. Chuchmarev: *Sov. Electrochem*., 1966, vol. 2, pp. 193-98.
56. R.J. Hundermark, S. Jahanshahi and S. Sun: *Proc. XXII Int. Mineral Processing Congr*., L. Lorenzen and D.J. Bradshow, eds., Cape Town, South Africa, 2003, South African Institute of Mining and Metallurgy, Johannesburg, South Africa, pp. 1370-77.
57. A. Adachi and K. Ogino: *Technol. Rep. Osaka Univ*., 1957, vol. 7 (224), pp. 121-26.
58. A. Adachi and K. Ogino: *Yoyuen (Fused Salt)*, 1961, vol. 1, p. 151.
59. V.W.A. Fischer and H.V. Ende: *Arch. Eisenhüttenwes*., 1951, vol. 22, pp. 417-22.
60. C. Gleitzer: *Key. Eng. Mater*., 1997, vol. 125–126, pp. 355-418.
61. N.F. Mott: *J. Non-Cryst. Solids*, 1968, vol. 1, pp. 1-17.
62. G.N. Greaves: *J. Non-Cryst. Solids*, 1973, vol. 11, pp. 427-46.